Influence of Co Doping on Structural and Band Gap Energy Properties of ZnO Based Varistor Ceramic

Ting Lee Mon[1], Nur Quratul Aini Ismail[1], Nor Kamilah Sa'at[1*], Raba' ah Syahidah Azis[1], Mohd Hafiz Mohd Zaid[1]

[1] Department of Physics, Faculty of Science, Universiti Putra Malaysia, Malaysia

Abstract: Photopyroelectric (PPE) technique has been widely used in applied science and technology fields including the study of materials in thermal and optical properties. The sample, $Zn_{1-x}Co_x$ (x= 0.4, 0.8, 1.2, 1.6, 2.0 wt%) was prepared using solid state method sintered at 1200℃ to study the effect of concentration on the energy band gap (E_g). XRD, SEM with EDX analysis were used to characterise the materials' structure, morphology, and density. The PPE setup is used to determine band gap energy (E_g) values. The E_g shows the decreasing trend when the concentration of CoO increases.

Keywords: Band gap energy; Solid-state method; Varistor Ceramic

Introduction

Zinc oxide (ZnO) is a white powder that is insoluble in water and widely use in materials and products such as rubber, plastics, ceramics, light emitting diodes, photodetectors, photodiodes, biosensors, gas sensors, solar cells, photocatalysis, active fillers, actuators and electromagnetic coupled sensors (Cruz et al., 2020; Keerthana & Kumar, (2020); Srivastava et al., 2013; Jiang et al, 2018; Mishra et al., 2017; Hahn, 2011). ZnO are widely use in semiconductors devices, ceramics such as varistor application (Billovits et al., 2021; Kołodziejczak-radzimska, & Jesionowski, 2014). Varistor are widely used as protective devices due to the highly nonlinear current voltage (I-V) characteristics. ZnO based varistor ceramics is formed by additives of metal oxide such as Bi_2O_3, Co_3O_4 and MnO. ZnO is use as major or base materials about 90 % because it has a wurtzite structure (Hafez, 2014). The O was arranged in a hexagonal close-packed type of lattice while Zn occupies half the tetrahedrals sites (Gupt, 1990). The ZnO has an open structure where external dopants easily enter the ZnO lattice. Co was chosen as dopants because the ionic radius of Co (0.65 Å) is smaller than Zn (0.74 Å). CoO

thin films are of interest with respect to numereous, such as optical sensors, magnetic detectors, catalytic membranes and optical gas sensors. It is used widely in ceramic industry as an additive to create blue coloured glazes and enamels.

Polyvinylidene diflouride (PVDF) has strong pyroelectric (PE) effect coefficient which has been discovered by Bergman et al. in 1971, stating that thermally induced current is proportional to the rate of change in temperature (Bergman et al., 1971). Due to the discovery of the PE property, PVDF has been widely applied especially uses of PVDF as the photopyroelectric (PPE) sensor. PVDF is inexpensive in cost, light in weight, and possesses excellent electrical characteristics. (Azmi et al., 2014), making PVDF a suitable sensor for the PPE technique.

The PPE technique has been widely used in applied science and technology fields, such as the study of materials' thermal and optical properties in single phase solids, liquids, gases, phase transitions, or combinations of these (Albuquerque et al., 2000; Bauer and Lang, 1996). Theory of the configuration of PPE technique presented by Mandelis et al. and the thermal diffusivity measurement of the optically opaque samples are done

_____
* Corresponding Author: kamilah@upm.edu.my

by Mandelis et al (1995) are applied in this study (Mandelis, & Shen, 1995). In standard PPE technique, the studied sample is in contact thermally with the sensor (in this study, the sensor is PVDF thin film) and the conductive grease as to reduce the thermal loss. The PPE technique is able to reject the sound interference from surroundings and response to thermal fluctuation (Zakaria et al., 2006). In this paper, the band gap energy (E_g) values of CoO doped ZnO with different concentration is studied by using PPE technique.

The measurement of PPE voltage is done by putting the samples on PVDF sensor in determining band gap energy (E_g) and it was assumed that the fundamental absorption edge of doped ZnO is due to the direct allowed transition. The optical absorption coefficient β varies with the excitation light energy hv and is given by the expression, $(\beta h\upsilon)^2 = C\ (h\upsilon - E_g)$ near the band gap, where hv is the photon energy, C is the constant independent of photon energy, and E_g is the direct allowed energy band-gap. The PPE signal intensity ρ is directly proportional to β, hence $(\rho h\upsilon)^2$ is related to hv linearly. The linear fitted region that crosses photon energy axis is extrapolated to determine the value of E_g (Zakaria et al., 2007).

In a study regarding the determination of thermal diffusivity, the measurement of thermal diffusivity, α involves the calculation of output voltage (V_0) of the PVDF sensor which is provided as (Marinelli et al., 1992).

$$\ln V_0 = K - \frac{\left(\frac{\pi f}{\alpha}\right)^{\frac{1}{2}}}{}\, l \tag{1}$$

where α is known as thermal diffusivity.
The gradient, m of the graph of $\ln V_0$ against cavity length, l and against square root frequency $\sqrt{f}$ plotted is equal to $-\sqrt{\frac{\pi f}{\alpha}}$. Thus, for the magnitude of α at a fixed value of frequencies is given by:

$$\alpha = \frac{\pi f}{m^2} \tag{2}$$

Likewise, the value for α or the specimen can be determined by changing the light source frequencies and fixed the cavity length, that is, frequency scanning method.
Based on equation 1:

$$\ln V_0 = K \,{}^{-l\left(\frac{\pi}{\alpha}\right)^{1/2}} f^{\frac{1}{2}} \tag{3}$$

The value gradient for the graph $\ln V_0$ against $\sqrt{f}$ plotted is $-l\sqrt{\frac{\pi}{\alpha}}$. Thus, the magnitude of α for the frequency scan can be shown as (Marinelli et al., 1992):

$$\alpha = \frac{\pi l^2}{m^2} \tag{4}$$

Method

Synthesis of sample

The sample of Co_x doped ZnO were prepared by using conventional solid state method (Ismail et al., 2020). The raw material of Co at different concentration of 0.4, 0.8, 1.2, 1.6, and 2.0 and ZnO are mixed together and undergo milling with zirconia balls for 24 h. The slurry was dried at 70 ˚C for 12 hours. Polyvinyl alcohol (PVA) solution 1.75 wt% was added to act as a binder to prevent the sample from crack and undergo grinding and sieving through 75 µm mesh screen. The samples were pressed with 1 tonne/m^2 pressure to form a pellet in 0.8 mm thickness. Those pellets are sintered at 1200 ˚C for 2 hours with heating and cooling rate of 5 ˚C/ min.

Structural study

The crystalline phase was identified using Cu Kα radiation (λ = 1.540598 Å) with PAnalytical X'Pert. XRD software X'Pert high score software Pro PW3040/60) was used to identify secondary phase and d-spacing. The d-spacing value was measured using Bragg's law:

$$n\lambda = 2d\ \sin\theta \tag{5}$$

Where λ is the wavelength of the x-ray incidents, n is the integer for number of order and d is the lattice spacing.

The crystal structure and crystallite size of the sample can be determined from XRD analysis. The crystallite size was calculated through the Debye-Scherer formula:

$$D = k\lambda\ /\ \beta\ \cos\theta \tag{6}$$

Where D is a crystallite size, k is a constant (approximately 0.89), λ is a wavelength of the incident beam, β is a full width at half maximum (FWHM) of the diffraction peak and θ is a Bragg reflection peak.

The microstructure and morphology of samples are observed by scanning electron microscope (SEM, model: JEOL 6400) attached with energy dispersive X-Ray (EDX). The average grain sizes (d) were determined by the linear intercept method, given by:

$$d = 1.56\ L/MN \tag{7}$$

where L is the random line length on the micrograph, M is the magnification of the micrograph, and N is the number of grain boundaries intercepted by the lines (Nahm, 2004):

The average density (ρ_{avg}) of sintered sample was measured by Archimedes method (Quratul et al., 2020):

$$\rho = W_{air}\rho_{diswater}\ /\ (W_{air} - W_{diswater}) \tag{8}$$

The sample was first weighed in air, W_{air}, and then immerse in distilled water, $W_{diswater}$. The weighing process was performed with an electronic balance. The estimated error was ±0.001 g cm⁻³.

The samples are then run by using a PPE setup as shown in Figure 1. The samples are put on top of PVDF sensor in which the sensor is connected to SR530 Lock-In Amplifier. The laser source chosen in this study is He-Ne blue laser (100mW, 473nm) of MBL-III-473. Thermal grease is applied to the lower surface of the sample as to reduce thermal loss during the experiment. The frequency of the chopper is fixed from 5 Hz to 20 Hz.
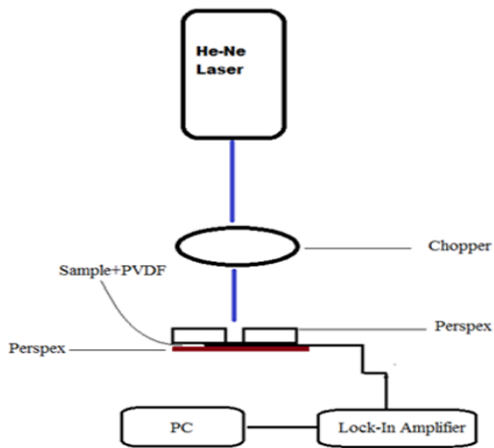

Figure 1. Schematic diagram of PPE setup.

Result and Discussion

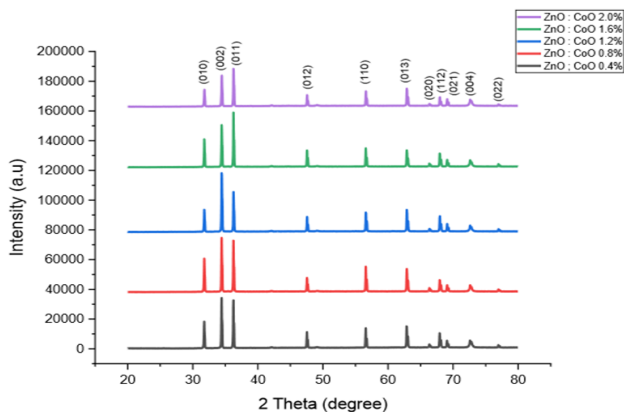*Analysis of Co doped ZnO structure*

Figure 2. XRD pattern of CoO doped ZnO at different concentration.

Figure 2 shows the XRD patterns of Co doped ZnO at five different concentrations of 0.4, 0.8, 1.2, 1.6 and 2.0 wt %. The XRD patterns of the samples showed discrete sharp peaks which reflected crystalline phase. The result shows that at the sharp peaks (011) the compounds are highly crystallized, where zincite phase is detected. At this phase, there is no secondary phase as the Co ions successfully occupy the lattice site (Caglar, 2013; Al-

Salman, & Abdullah, 2013). The flipped in peak intensity of ZnO in between (0 1 1) plane and (0 0 2) plane is due to the Co ions in the lattice site effect the growth of ZnO. Shinde et al., (2006) states undoped ZnO has high peak intensity of (0 0 2) plane compare to the Mn doped ZnO where the high peak intensity flipped from (0 0 2) plane to (1 0 1) plane due to the Mn ions may act as obstacle for the growth of ZnO along (0 0 2) during deposition of ZnO. It is seen that the decreasing of the peak intensity as increase the Co concentration is confirmed due to the degradation of the crystallinity. The peak (002) is clearly seen the lower intensities as the diffusion of Co ions into the Zn^{2+} sites induce a crystal defect because of the difference in ion size between cobalt (Co) and Zinc (Zn). The diffusion of Co ions occurs as Co^{2+} (0.65 Å) has smaller ions compare to the Zn^{2+} (0.74 Å) as mentioned above. This resulting the defect change in the stoichiometry of the ZnO lattice. The decreasing in the peak intensity as increasing Co concentration also agreed by the Caglar (2013) reported decrease in the peak intensity observed in the XRD patterns as increase in the Co concentration.

SEM Analysis

SEM analysis is conducted to study the average grain size, shape and morphology of the sintered sample. Figure 3 shows the microstructure of the different concentrations of CoO doped ZnO sintered at 1200 ˚C. In general, the grain size of the samples increases as the Co concentration increases, which also in agreement to Wang et.al (2011). The following average grain size is calculated from the micrograph using lineal intercept technique: (a) 0.0294 μm for the 0.4 wt % of CoO, (b) 0.050 μm for the 1.2 wt % of CoO and (c) 0.0347 μm for the 2 wt % of CoO. The porosity of sintered sample decreases when the CoO concentration is increased from 0.4 wt % to 2.0 wt %. Samples of 1.2 wt% CoO fluctuates with the largest average grain size of 0.050μm may due to the less porosity resulting in more compact of the sample structure.
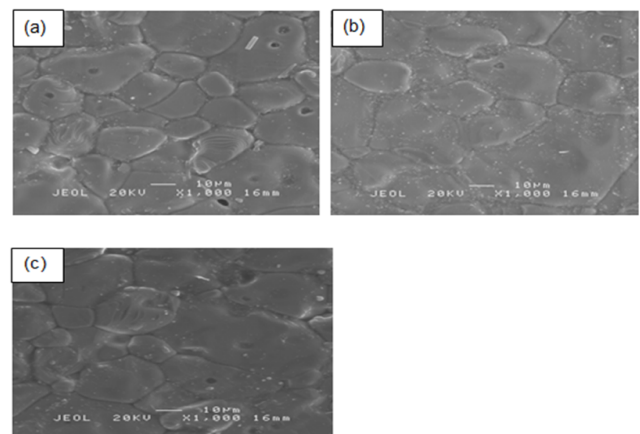

Figure 3. SEM micrographs with different CoO concentration sintered at 1200 ˚C for 2 h: (a) 0.4 wt % CoO, (b) 1.2 wt % of CoO and (c) 2 wt % CoO.
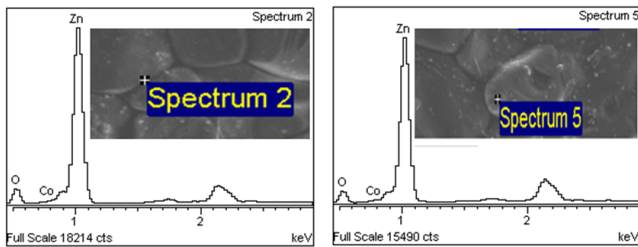
Figure 4. EDX of the 2 wt % CoO concentration.

Spectrum	O	Co	Zn	Total
2	12.09	1.02	86.89	100.00
5	8.88	1.00	90.12	100.00

Figure 4 shows the EDX analysis for the 2 wt % of CoO concentration. The grain boundary of ZnO confirmed contain CoO element as shown in spectrum 2 and spectrum 5 which reflects that CoO was diffused in the grain of ZnO. This is due to the smaller ionic size of Co which is 0.65 Å while 0.74 Å.

Density

Table 1: Density of samples of different concentration CoO.

Samples	CoO concentration (wt %)	Density (gcm^{-3})
1	0.4	5.312
2	0.8	5.624
3	1.2	5.805
4	1.6	5.667
5	2.0	5.687

Based on the tabulated data in Table 1, the density of pellet CoO doped ZnO increases as CoO concentration is increased which also consistent with other report (Hamdelou, 2014). The increase in density is due to the fact that Zn has higher atomic size compared to Co. When the concentration of Co increases, the Co atom diffuses to the ZnO sample, which in turn making the density of the sample to increase.
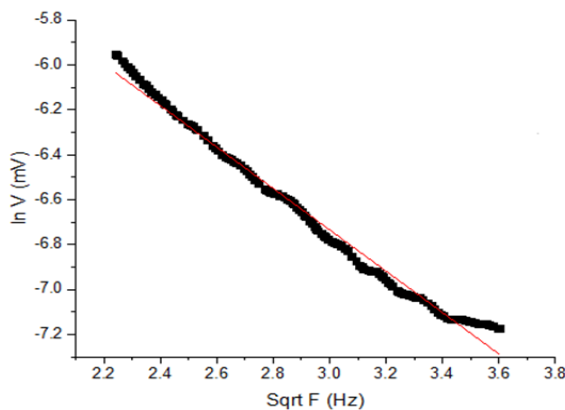
Thermal diffusivity

Figure 5. Graph of ln V (mV) against square root frequency (Hz) of 1.6% CoO.
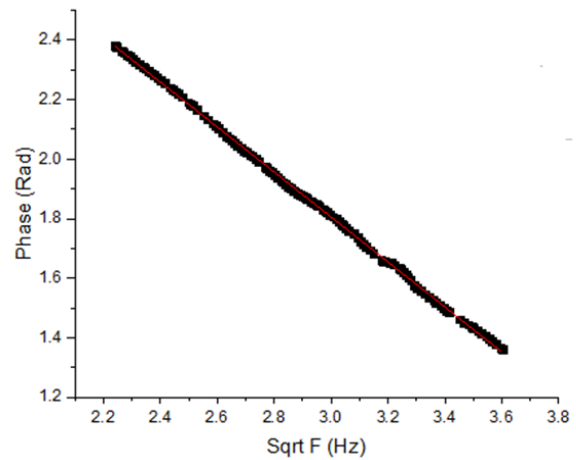

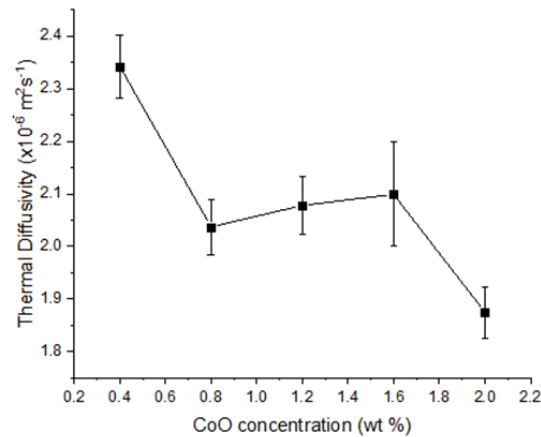**Figure 6.** Graph of phase against square root of frequency of 1.6% CoO.

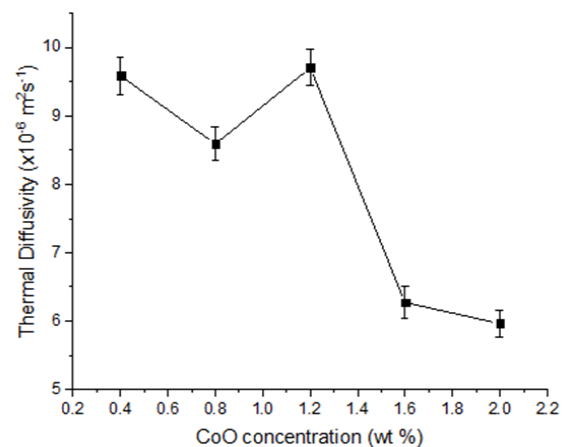**Figure 7.** Thermal diffusivity of different CoO concentration using voltage signal.

**Figure 8.** Thermal diffusivity of different concentration of CoO using phase signal.

Figure 5 and 6 show the experimental results obtained for dopant concentration of 1.6% It is shown that the ln V has more accurate and consistent result if

compared to that of phase signal. From Figure 7 and 8 (by applying equation (4)), thermal diffusivity of shows a decreasing trend with increasing concentration of CoO generally. However, the decrease in thermal diffusivity with the increasing of the CoO concentration is predicted by Equation (1) as α is inversely proportional to ρ (Adek, 2008). We notice that the thermal diffusivity values are in the range of Mn doped ZnO of (2.139 ± 0.002) x 10^{-6} m²s⁻¹ and Cu doped ZnO of (3.46 ± 0.02) x 10^{-6} m²s⁻¹ (Rabiatuladawiyah, & Zaidan, 2015; Mishra et al., 2015). The thermal diffusivity values obtained by using phase signal has a greater deviation compared to that of using voltage signal may due to the process when output signal is sent to lock-in which caused much deviation in phase signal. However, both of the experimentally determined thermal diffusivity results showing decrement when increasing density.

Band gap energy (E$_g$)
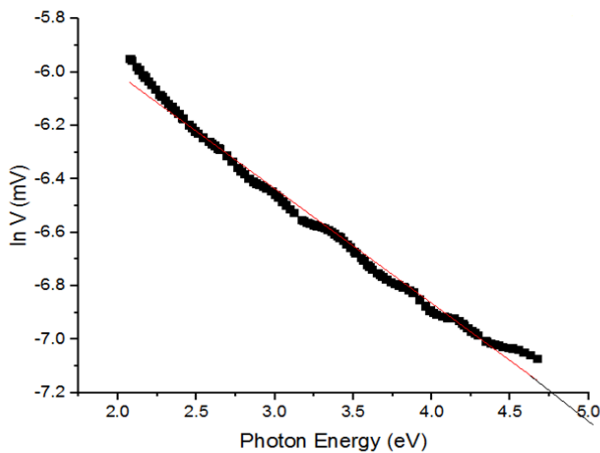
Figure 9. Graph of ln V against Photon Energy (eV) for concentration 1.6 wt % of CoO.
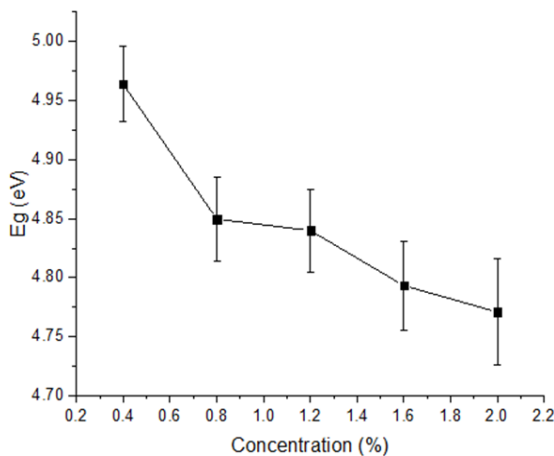
Figure 10. Graph of Eg (eV) against concentration of CoO.

Figure 9 shows the band gap energy (Eg) is determined by extrapolating the plot of ln V vs photon energy to the x-axis, which was explained in previous section. From Figure 10, it can be clearly seen that when the concentration of CoO increases, the band gap energy (Eg) shifts to lower energy (redshift) which indicates the high successful incorporation of Co2+ into Zn2+ lattice during liquid phase sintering process. However, the broader Eg than the common pure ZnO of ~3.4 eV probably due to thick sample of 1mm as well as inhomogeneities (defects) from impurities of Co in the ZnO lattice structure which introduces a large loss absorption during the optical absorption edge (Mishra et al., 2015; Joshi et al., 2016; Kumar et al., 2014). The presence of dopant generated an absorption profile within the band tail in conduction and valence band is explained in terms of Urbach energy (Eu) that is originated from structural disorders, compositional fluctuations, point defects, grain boundaries, and strain (Kumar et al., 2014). The higher the percentage of dopant concentration the larger the degree of structural disorder, thus increased the tail width of localized electronic state and resulting of the narrow the Eg (redshift) which consistent with density, SEM and XRD results with indicates the presence of interface state due to the doping of CoO in ZnO ceramic varistor.

Conclusion

Throughout this study, when concentration of CoO increases, band gap energy (Eg) values decreases gradually, the peak intensity in XRD decreases and the porosity of sample decreases. The shift of band gap energy (Eg) to a lower energy is consistent with the results of XRD, SEM with EDX analysis and density. The reduction of peak intensity as increasing Co concentration due to the diffusion of Co2+ into the Zn lattice structure which caused the increase of grain size and compactness of the Co doped ZnO ceramic varistor. The increase of Co dopant in the ZnO varistor ceramic is responsible to the increase of structural disorder that narrowing Eg to the lower energy (redshift). Thermal diffusivity values obtained in the range of (2.342±0.060) x 10-6 m2s-1 to (1.875±0.049) x 10-6 m2s-1 and comparable to thermal diffusivity values of Mn doped ZnO (2.139 ± 0.002) x 10-6 m2s-1 and Cu doped ZnO (3.46 ± 0.02) x 10-6 m2s-1 which indicates the effect of dopant and the larger the density of the Co doped ZnO, the lower the thermal diffusivity.

Acknowledgements

Compliance with Ethical Standards

References

Adek, N.N.N. (2008). Measurement of Thermal Diffusivity of Ceramics (ZnO) Doped with MnO and Dy2O3 by Using Photoflash Technique (*Doctoral dissertation, Universiti Putra Malaysia*).

Akhir, R., & Wahab, zaidan. (2015). Thermal diffusivity studies of ZnO-CuO at high temperatures. *Jurnal Teknologi*, *76*, 19–23. https://doi.org/10.11113/jt.v76.5505

Al-Salman, H. S., & Abdullah, M. J. (2013). Fabrication and characterization of undoped and cobalt-doped ZnO based UV photodetector prepared by RF-sputtering. *Journal of Materials Science & Technology*, 29(12), 1139-1145.

Azmi, B. Z., Liaw, H. S., Yunus, W. M. M., Hashim, M., Moksin, M. M., & Yusoff, W. M. D. W. (2004). Normalisation procedure in thermal wave approach of thermal diffusivity measurement of solids using pyroelectric sensor. *Infrared Physics & Technology*, *45*(4), 315–321. https://doi.org/https://doi.org/10.1016/j.infrared.2004.01.002

Bauer, S., & Lang, S. B. (1996). Pyroelectric polymer electrets. *IEEE Transactions on Dielectrics and Electrical Insulation*, *3*(5), 647–676. https://doi.org/10.1109/94.544186

Bergman, J. G., McFee, J. H., & Crane, G. R. (1971). PYROELECTRICITY AND OPTICAL SECOND HARMONIC GENERATION IN POLYVINYLIDENE FLUORIDE FILMS. *Applied Physics Letters*, *18*(5), 203–205. https://doi.org/10.1063/1.1653624

Billovits, T., Kaufmann, B., & Supancic, P. (2021). Measurement of the piezotronic effect on single grain boundaries in zinc oxide Varistors. *Open Ceramics*, *6*, 100125. https://doi.org/https://doi.org/10.1016/j.oceram.2021.100125

Caglar, Y. (2013). Sol – gel derived nanostructure undoped and cobalt doped ZnO：Structural , optical and electrical studies. *Journal of Alloys and Compounds*, *560*, 181–188. https://doi.org/10.1016/j.jallcom.2013.01.080

Caglar, Y. (2013). Sol–gel derived nanostructure undoped and cobalt doped ZnO: Structural, optical and electrical studies. *Journal of alloys and Compounds*, 560, 181-188.

De Albuquerque, J. E., Melo, W. L. B., & Faria, R. M. (2000). Photopyroelectric spectroscopy of polyaniline films. *Journal of Polymer Science Part B: Polymer Physics*, *38*(10), 1294–1300. https://doi.org/https://doi.org/10.1002

Gupta, T. (2005). Application of ZnO Oxide Varistors. *Journal of the American Ceramic Society*, *73*, 1817–1840. https://doi.org/10.1111/j.1151-2916.1990.tb05232.x

Hafez, A. (2014). *Development of Enhanced Hydrogen-Doped Indium Oxide Material Properties by Integration of a Negatively Biased Mesh into the Sputtering Process*. https://doi.org/10.6084/m9.figshare.1368242.v1

Hahn, Y.-B. (2011). Zinc oxide nanostructures and their applications. *Korean Journal of Chemical Engineering*, *28*(9), 1797. https://doi.org/10.1007/s11814-011-0213-3

Hamdelou, S., Guergouri, K., & Arab, L. (2014). The effect of the starting powders particle size on the electrical properties of sintered Co doped ZnO varistors. *Applied Nanoscience*, *5*, 1–9. https://doi.org/10.1007/s13204-014-0382-6

Ismail, N., Saat, N., & Mohd Zaid, M. (2020). Enhancement of Non-Ohmic Properties of CoO DopeD ZnO Varistor Ceramics using Soda Lime Silica (SLS) Glass. *Sains Malaysiana*, *49*, 871–876. https://doi.org/10.17576/jsm-2020-4904-16

Joshi, K., Rawat, M., Gautam, S. K., Singh, R. G., Ramola, R. C., & Singh, F. (2016). Band gap widening and narrowing in Cu-doped ZnO thin films. *Journal of Alloys and Compounds*, *680*, 252–258. https://doi.org/https://doi.org/10.1016/j.jallcom.2016.04.093.

Keerthana, S., & Kumar, A. (2020). Potential risks and benefits of zinc oxide nanoparticles: a systematic review. *Critical Reviews in Toxicology*, *50*(1), 47–71. https://doi.org/10.1080/10408444.2020.1726282

Kołodziejczak-Radzimska, A., & Jesionowski, T. (2014). Zinc Oxide—From Synthesis to Application: A Review. In *Materials* (Vol. 7, Issue 4). https://doi.org/10.3390/ma7042833

Kumar, S., Sharma, P., & Sharma, V. (2014). Red Shift in Absorption Edge of Cd1-xCoxS Nanofilms. *IEEE Transactions on Nanotechnology*, *13*, 343.

Liu, D.-M. (1996). Effect of specimen thickness on the thermal diffusivity of (Sr, K)Zr4(PO4)6 ceramic via a laser-flash technique. *Journal of Materials Science*, *31*(1), 86–89. https://doi.org/10.1007/BF00355130

Marinelli, M., Zammit, U., Mercuri, F., & Pizzoferrato, R. (1992). High-resolution simultaneous photothermal measurements of thermal parameters at a phase transition with the photopyroelectric technique. *Journal of Applied Physics*, *72*(3), 1096–1100. https://doi.org/10.1063/1.351785

Medina Cruz, D., Mostafavi, E., Vernet-Crua, A., Barabadi, H., Shah, V., Cholula-Díaz, J. L., Guisbiers, G., & Webster, T. J. (2020). Green nanotechnology-based zinc oxide (ZnO) nanomaterials for biomedical applications: a review. *Journal of Physics: Materials*, 3(3), 34005. https://doi.org/10.1088/2515-7639/ab8186

Mishra, P. K., Mishra, H., Ekielski, A., Talegaonkar, S., & Vaidya, B. (2017). Zinc oxide nanoparticles: a promising nanomaterial for biomedical applications. *Drug Discovery Today*, 22(12), 1825–1834. https://doi.org/https://doi.org/10.1016/j.drudis.2017.08.006

Mishra, R., Militky, J., & Venkataraman, M. (2019). 7 - Nanoporous materials. In R. Mishra & J. B. T.-N. in T. Militky (Eds.), *The Textile Institute Book Series* (pp. 311–353). Woodhead Publishing. https://doi.org/https://doi.org/10.1016/B978-0-08-102609-0.00007-9

Nahm, C.-W. (2004). Effect of cooling rate on degradation characteristics of $ZnO \cdot Pr6O11 \cdot CoO \cdot Cr2O3 \cdot Y2O3$-based varistors. *Solid State Communications*, 132(3), 213–218. https://doi.org/https://doi.org/10.1016/j.ssc.2004.07.040.

Quratul, N., Ismail, A., Saat, N. K., Hafiz, M., & Zaid, M. (2020). Effect of soda lime silica glass doping on ZnO varistor ceramics : dry milling method. Journal of Asian Ceramic Societies, *Journal of Asian Ceramic Societie.* 00(00), 1–6. https://doi.org/10.1080/21870764.2020.1793472

Shen, J., & Mandelis, A. (1995). Thermal-wave resonator cavity. *Review of Scientific Instruments*, 66(10), 4999–5005. https://doi.org/10.1063/1.1146123

Shinde, V., Gujar, T., Lokhande, C., Mane, R., & Han, S.-H. (2006). Mn doped and undoped ZnO films: A comparative structural, optical and electrical properties study. *Materials Chemistry and Physics*, 96, 326–330. https://doi.org/10.1016/j.matchemphys.2005.07.045.

Srivastava, V., Gusain, D., & Sharma, Y. C. (2013). Synthesis, characterization and application of zinc oxide nanoparticles (n-ZnO). *Ceramics International*, 39(8), 9803–9808. https://doi.org/https://doi.org/10.1016/j.ceramint.2013.04.110

Wang, M., Li, G., & Yao, C. (2011). Microstructure and electrical properties of Pr6O11–Co3O4–MnCO3–Y2O3-doped ZnO varistors. Ceramics International, 37(7), 2901–2905. https://doi.org/10.1016/j.ceramint.2011.03.076

Zakaria, A., Rizwan, Z., Halim, S. A., Yunus, W. M. M., & Hashim, M. (2007). Photothermal Study of ZnO Ceramic Doped With TiO2, *Solid State Science and Technology.* 15(2), 34–43.

Zakaria, A., Sang, L. H., Abbas, Z., Yunus, W. M. M., & Hassan, J. (2006). Measurement of thermal parameter using non-contact photopyroelectric method. *ScienceAsia*, 32(1), 47–52. https://doi.org/10.2306/scienceasia1513-1874.2006.32.047